Supplementary Information

SECTION S1: PROPOSED MODEL FOR INDUCTION AND SHUTDOWN OF THE CONJUGATION OPERON IN PAD1 AND PAM373.

Based on the organizational similarity, the model previously developed for pCF10 signalling system was adopted for the pheromone controlled conjugation in pAD1 and pAM373. Plasmid pAD1 has a very high similarity with pCF10 in the potency of the inducing signalling peptide. We thus postulated that the regulation of induction of the conjugation operon of pAD1 is very similar to pCF10. The binding constants of both the peptides to TraA are set to the same value (10^{-12}-10^{-13} M) as in pCF10 system (Table S2). Due to such high binding constants, the peptides bound to TraA remain bound until degradation. Further, the binding affinities of peptide-TraA complexes with the operator are also set to be identical as in pCF10 (10^{-11} M) which is three orders of magnitude higher than apo-TraA binding to the operator site (10^{-8} M). Under uninduced conditions, apo-TraA is predominant and a few TraA-iAD1 complexes are formed due to basal leaky expression of iAD1. These apo-TraA and TraA-iAD1 complexes occupy the binding sites in the plasmid pAD1, repressing the P_O promoter and supressing the expression of the conjugation operon. The presence of extracellular cAD1 causes its import and binding to apo-TraA, forming TraA-cAD1 complexes. The high affinity TraA-cAD1 tetramers bind to the operator and displace the apo-TraA/DNA complexes, leading to de-repression of the P_O promoter and induction of the conjugation operon. Induction then leads to increased production of iAD1, which is processed and exported into the growth medium. The iAD1 peptide, an indicator for donor density, is imported and binds to apo-TraA, forming large amount of repressing TraA-iAD1 complexes. These complexes displace TraA-cAD1 bound to the operator sites in the plasmids and shut down the expression of conjugation operon (Figure S5A).

In the case of pAM373, the concentration of cAM373 required for induction is much higher than in the pCF10 and pAD1 systems, suggesting that the binding affinities involved are very different from those two systems. Lumping the binding events, i.e. the binding affinities of peptides with TraA and the subsequent binding of the TraA complexes with the operator site, one obtains an equation relating gene expression to the combined binding events (Eq. S9). From the order of magnitude estimate we expect that $K_{O-A_4C_4}K_{A-C}$ would be about 100-fold lower than in pCF10 and pAD1 systems. We evaluated two scenarios: the affinity of peptide binding to TraA is two orders of magnitude higher while the binding of the TraA complexes with the operator is unchanged, and vice versa. We then simulated both these scenarios to examine which of the two cases represents experimentally observed induction kinetics.

For the first case we set the binding constants of peptides to TraA differing by 100-fold ($K_{A-C} \approx 1\times10^{11} M^{-1}, K_{A-I} \approx 1\times10^{13} M^{-1}$) and the binding constants of the TraA complexes to the operator site as shown in Table S2 (Parameter set I). From the concentration profiles of the various species, we see the high expression of *traE* which does not show a fast shut down seen as in experiments (Figure S5B). This is because the concentration of TraA-cAD1 complexes is high and there are not enough TraA-iAD1 complexes to shut down the expression of *traE*.

Next we simulated the case where we set the binding constants of TraA complexes to the operator sites as shown in Table S2 (Parameter set II). Under this parameter set, we were able to recapitulate the induction behaviour of the conjugation operon qualitatively (Figure S5C). As seen from experiments, a high induction concentration of cAM373 would result in high intracellular concentration of TraA-cAM373. High levels of TraA-cAM373 complexes out-compete apo-TraA complexes for binding to the operator, ultimately resulting in induction. Upon induction, the iAM373 concentration increases rapidly, thus increasing the intracellular TraA-iAM373

concentration. Higher affinity of TraA-iAM373 to the operator site ($K_{O-A_4I_4} = 1\times10^{11} M^{-1}$ vs. $K_{O-A_4C_4} = 1\times10^{9} M^{-1}$) leads to shutting down of the transcription of the operon rapidly. It is likely that the binding characteristics in cAM373 is closer to the second scenario.

REFERENCES

[1] Chatterjee, A., Cook, L. C. C., Shu, C. C., Chen, Y. Q., Manias, D. A., Ramkrishna, D., Dunny, G. M., and Hu, W. S. (2013) Antagonistic self-sensing and mate-sensing signaling controls antibiotic-resistance transfer, *P Natl Acad Sci USA 110*, 7086-7090.

SECTION S2: OBTAINING ORDER OF MAGNITUDE ESTIMATES FOR BINDING CONSTANTS FOR USE IN MATHEMATICAL MODEL

The general mechanism considered is depicted in Figure S4. The binding events are summarized in the reactions below. Applying rapid equilibrium assumption and pseudo-first order reactions with respect to each reactant, we obtain the following relationships.

$$2A_2 + 4C \xrightleftharpoons{K_{A-C}} A_4C_4, \quad [A_4C_4] = K_{A-C}[A_2][C] \tag{S1}$$

$$2A_2 + 4I \xrightleftharpoons{K_{A-I}} A_4I_4, \quad [A_4I_4] = K_{A-I}[A_2][I] \tag{S2}$$

$$O + 2A_2 \xrightleftharpoons{K_{O-A_2}} OA_4, \quad [OA_4] = K_{O-A_2}[O][A_2] \tag{S3}$$

$$O + A_4C_4 \xrightleftharpoons{K_{O-A_4C_4}} OA_4C_4, \quad [OA_4C_4] = K_{O-A_4C_4}[O][A_4C_4] \tag{S4}$$

$$O + A_4I_4 \xrightleftharpoons{K_{O-A_4I_4}} OA_4I_4, \quad [OA_4I_4] = K_{O-A_4I_4}[O][A_4I_4] \tag{S5}$$

The net sum of repressed and induced forms of DNA would equal the copy number of the plasmid as shown in Eq. S6, where [N] is the concentration of plasmid in the donor cell.

$$[N] = [O] + [OA_4] + [OA_4C_4] + [OA_4I_4] \tag{S6}$$

Substituting Eqs. S1-S6 in S7 we can obtain the following relationships

$$[N] = [O] + K_{O-A_2}[O][A_2] + K_{O-A_4C_4}K_{A-C}[O][A_2][C] + K_{O-A_4I_4}K_{A-I}[O][A_2][I] \tag{S7}$$

$$[O] = \frac{[N]}{1 + K_{O-A_2}[A_2] + K_{O-A_4C_4}K_{A-C}[A_2][C] + K_{O-A_4I_4}K_{A-I}[A_2][I]} \tag{S8}$$

$$[OA_4C_4] = \frac{K_{O-A_4C_4}K_{A-C}[A_2][C][N]}{1 + K_{O-A_2}[A_2] + K_{O-A_4C_4}K_{A-C}[A_2][C] + K_{O-A_4I_4}K_{A-I}[A_2][I]} \tag{S9}$$

At the induction, the effect of *I* can be assumed to be negligible, hence the third term in the denominator is dropped. For induction we expect that atleast one of the plasmids is bound by A_4C_4.

Hence LHS of Eq. S9 has a value of 1, so $K_{O-A_4C_4}K_{A-C}[A_2][C][N] >> K_{O-A_2}[A_2] > 1$. The full induction is thus dependent on $K_{O-A_4C_4}K_{A-C}[C] >> K_{O-A_2}$.

In the case of pAD1, C for induction is small ($C \sim 10^{-9}$M). K_{O-A_2} was estimated to be 10^8 M^{-1}. The value of $K_{O-A_4C_4}$ and K_{A-C} used for pAD1 (adopted from those for pCF10; Table S2) indeed meet the condition of $K_{O-A_4C_4}K_{A-C}[C] >> K_{O-A_2}$. Upon the induction and the accumulation of the inhibitor peptide, the transcription rate from O is suppressed. The last term in the denominator in Eq. S9 becomes dominating. The high transcript level of inhibitor peptide upon induction puts $[C]/[I] \approx 1$, which gives an order-of-magnitude estimate for the ratio of kinetic constants to the value used in the model for pCF10 (and is adopted for pAD1 in this study) as

$$\frac{K_{O-A_4I_4}K_{A-I}}{K_{O-A_4C_4}K_{A-C}} \approx 1 \qquad \text{(S10)}$$

For pAM373, C is much larger, $\sim 10^{-6}$-10^{-7} M range. Given the same value of K_{O-A_2}, the value of $K_{O-A_4C_4}K_{A-C}[C]$ will be 100 times smaller than that of pAD1. The reduction in the value can be realized either in K_{A-C} or in $K_{O-A_4C_4}$ (Table S2). For the parameter values involved in the inhibitor peptide, the same set of values as those used for pCF10 were used (Table S2).

Supplementary Tables and Figures

Table *S1*: Common features of the family of conjugative plasmids.

Function	Proteins and relevant genes involved in conjugation steps in different plasmids		
	pCF10	pAD1	pAM373
Secretion of chromosomally-encoded sex pheromone	cCF10 (*ccfA*)	cAD1 (*cad*)	cAM373 (*camE*)
Inhibitor of conjugation	iCF10 (*prgQ*)	iAD1 (*iad1*)	iAM373 (*iAM373*)
Recognition and internalization of pheromone	PrgZ	TraC	TraC
Sequestration of endogenous pheromone	PrgY	TraB	-
Regulator of conjugation system	PrgX	TraA	TraA
Synthesis of aggregation substance (AS)	PrgB	Asa1	Asa373
Surface exclusion protein	PrgA	Sea1	-

Table S2: Binding constants used in the mathematical model to fit the kinetics of induction

Reaction	Equilibrium Constant	pAD1	pAM373	
			Parameter set I	Parameter set II
$2A_2 + 4C \xrightleftharpoons{K_{A-C}} A_4C_4$	$K_{A-C} = \frac{[A_4C_4]}{[A_2][C]}$	$1\times10^{13} M^{-1}$	$1\times10^{11} M^{-1}$	$1\times10^{13} M^{-1}$
$2A_2 + 4I \xrightleftharpoons{K_{A-I}} A_4I_4$	$K_{A-I} = \frac{[A_4I_4]}{[A_2][I]}$	$1\times10^{13} M^{-1}$	$1\times10^{13} M^{-1}$	$1\times10^{13} M^{-1}$
$O + 2A_2 \xrightleftharpoons{K_{O-A_2}} OA_4$	$K_{O-A_2} = \frac{[OA_4]}{[O][A_2]}$	$1\times10^{8} M^{-1}$	$1\times10^{8} M^{-1}$	$1\times10^{8} M^{-1}$
$O + A_4C_4 \xrightleftharpoons{K_{O-A_4C_4}} OA_4C_4$	$K_{O-A_4C_4} = \frac{[OA_4C_4]}{[O][A_4C_4]}$	$1\times10^{11} M^{-1}$	$1\times10^{11} M^{-1}$	$1\times10^{9} M^{-1}$
$O + A_4I_4 \xrightleftharpoons{K_{O-A_4I_4}} OA_4I_4$	$K_{O-A_4I_4} = \frac{[OA_4I_4]}{[O][A_4I_4]}$	$1\times10^{11} M^{-1}$	$1\times10^{11} M^{-1}$	$1\times10^{11} M^{-1}$

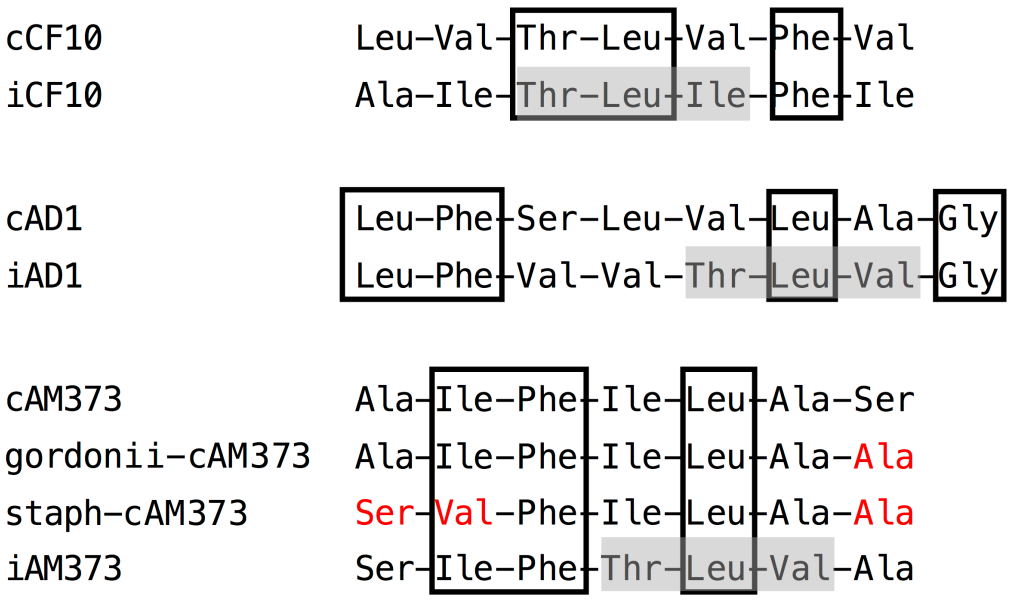

Figure S1: Amino acid sequences of *E. faecalis* pheromones and inhibitors. The boxed residues show the structure similarity between pheromone and inhibitor. Thr-Leu-Val/Ile residues in the inhibitor peptide sequences indicate the conservation of structure similarity within the inhibitor.

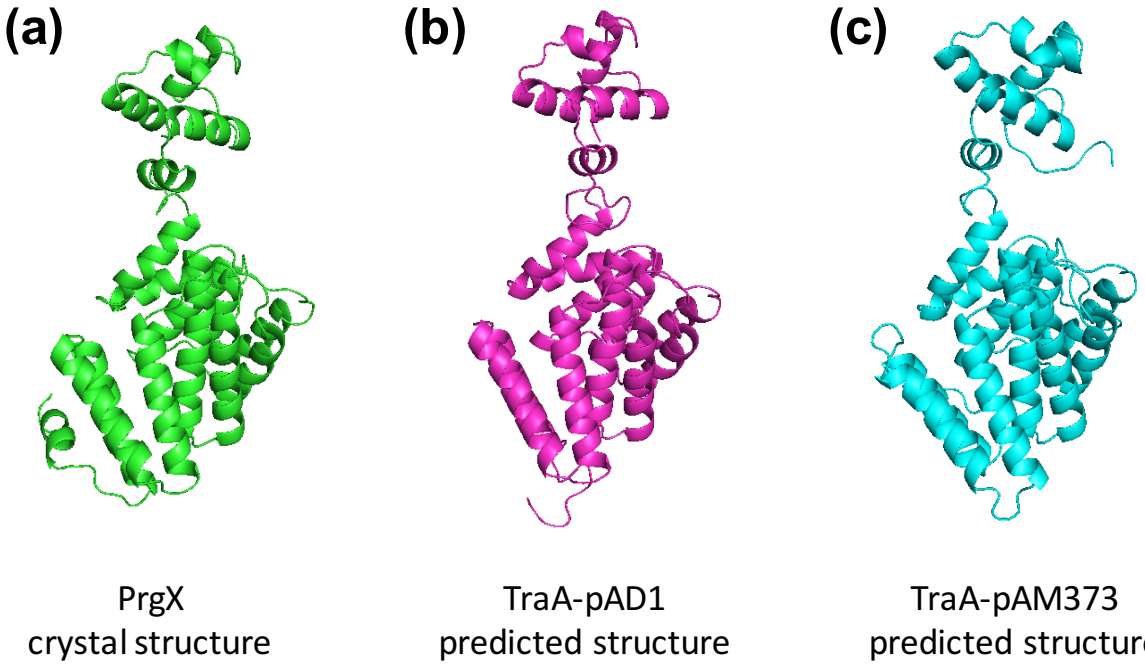

Figure S2: Structure of regulatory proteins. (a) Crystal structure of PrgX encoded in pCF10 (green). (b) Predicted structure of TraA encoded in pAD1 (magenta). (c) Predicted structure of TraA encoded in pAM373 (cyan).

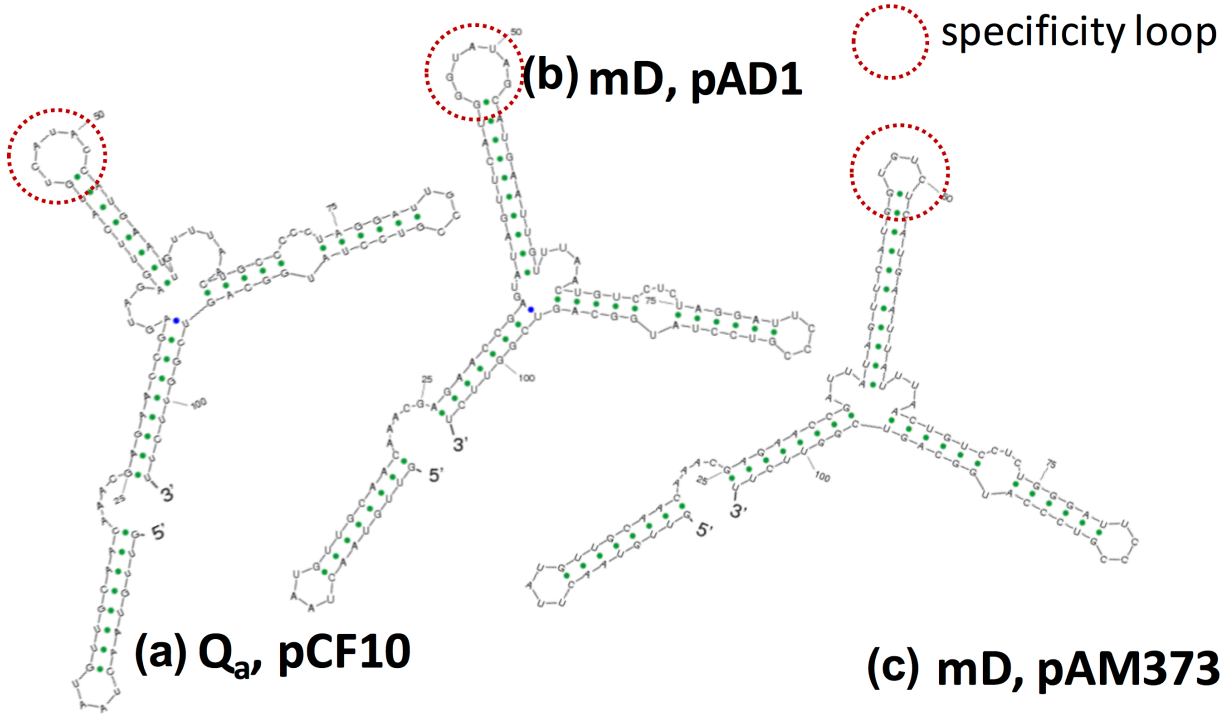

Figure S3: Predicted secondary structures of regulatory sRNAs. (a) Qa in pCF10, (b) mD in pAD1 and, (c) mD in pAM373.

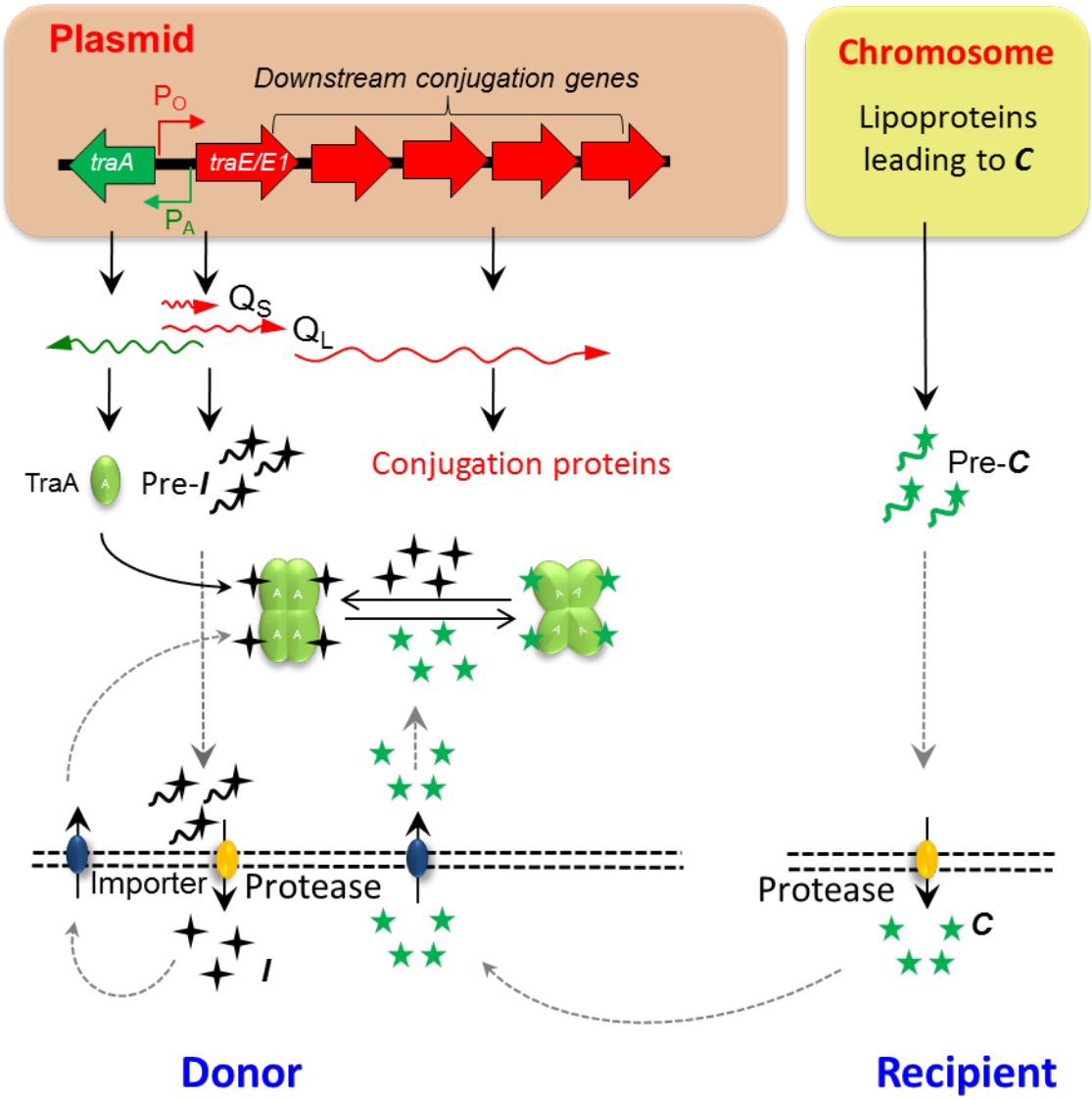

Figure S4: Control of conjugation by two antagonistic peptide signals in *E. faecalis*. Signaling molecules C and I are processed and released by recipient and donor cells, respectively, and imported into the donor cell, where these signals compete for binding to TraA. TraA and TraA-I complexes repress the P_o promoter driving the conjugation operon whereas TraA-C complexes induce the P_o promoter. In uninduced donor cells, basal transcription of though the P_o promoter generates a short-transcript (Q_S) encoding the inhibitor. Induced cells express extended transcripts encoding *traE/E1* and other conjugation genes

(A)

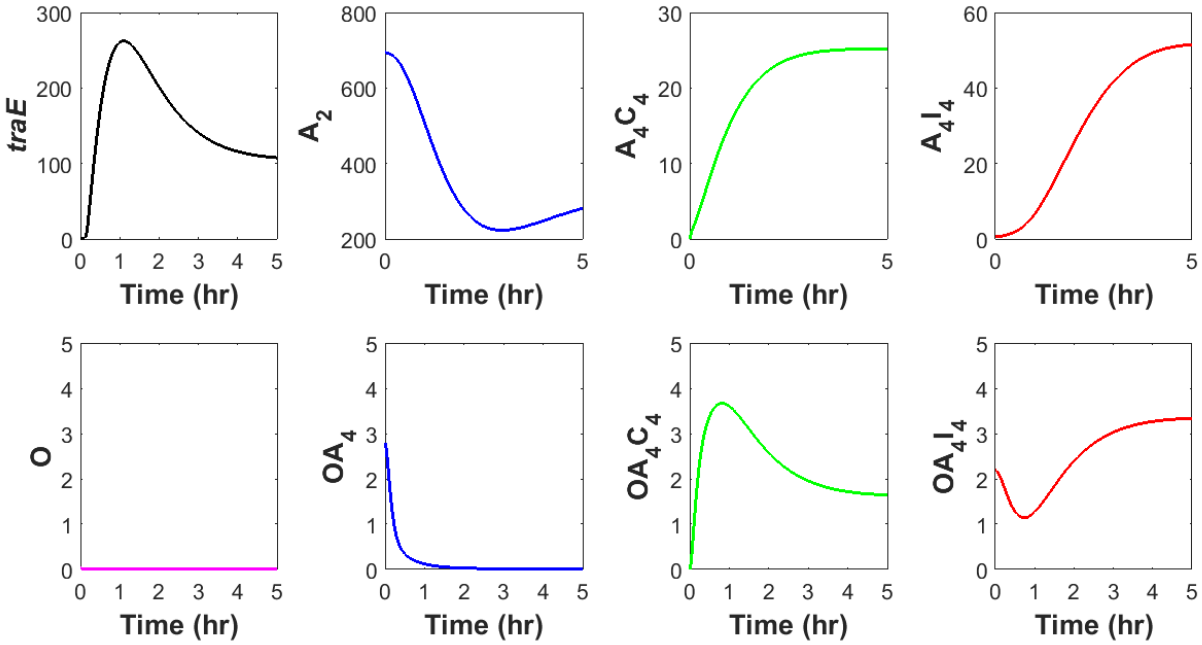
traE
A2
A4C4
A4I4
O
OA4
OA4C4
OA4I4
Time (hr)

(B)

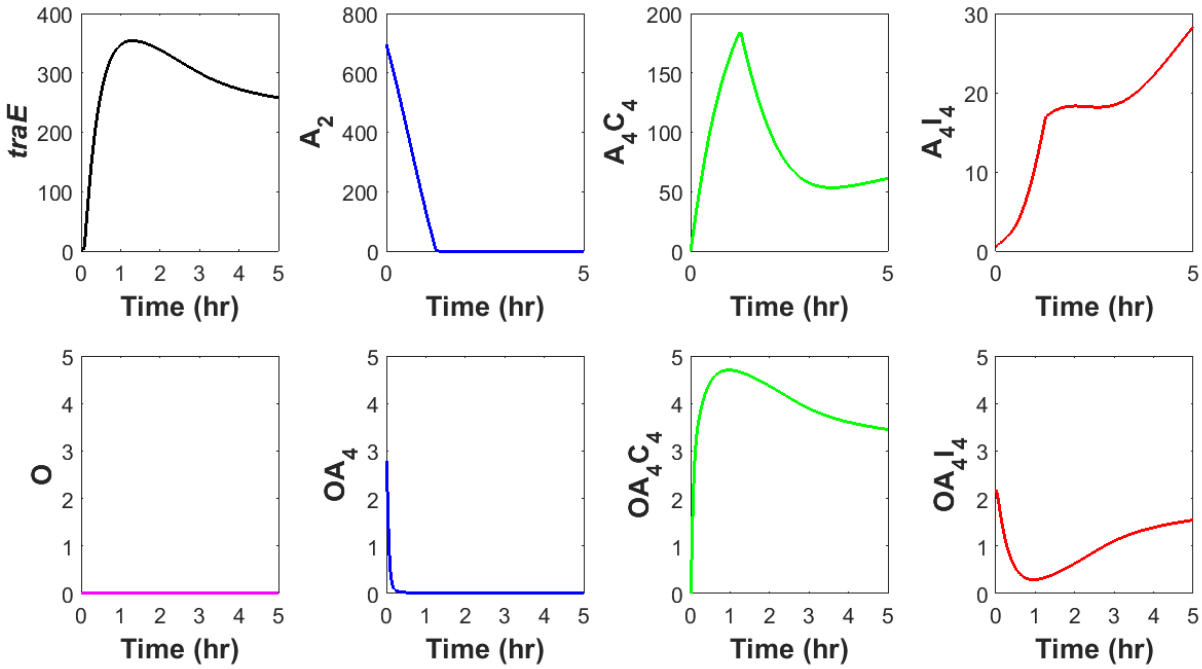
traE
A2
A4C4
A4I4
O
OA4
OA4C4
OA4I4
Time (hr)

(C)

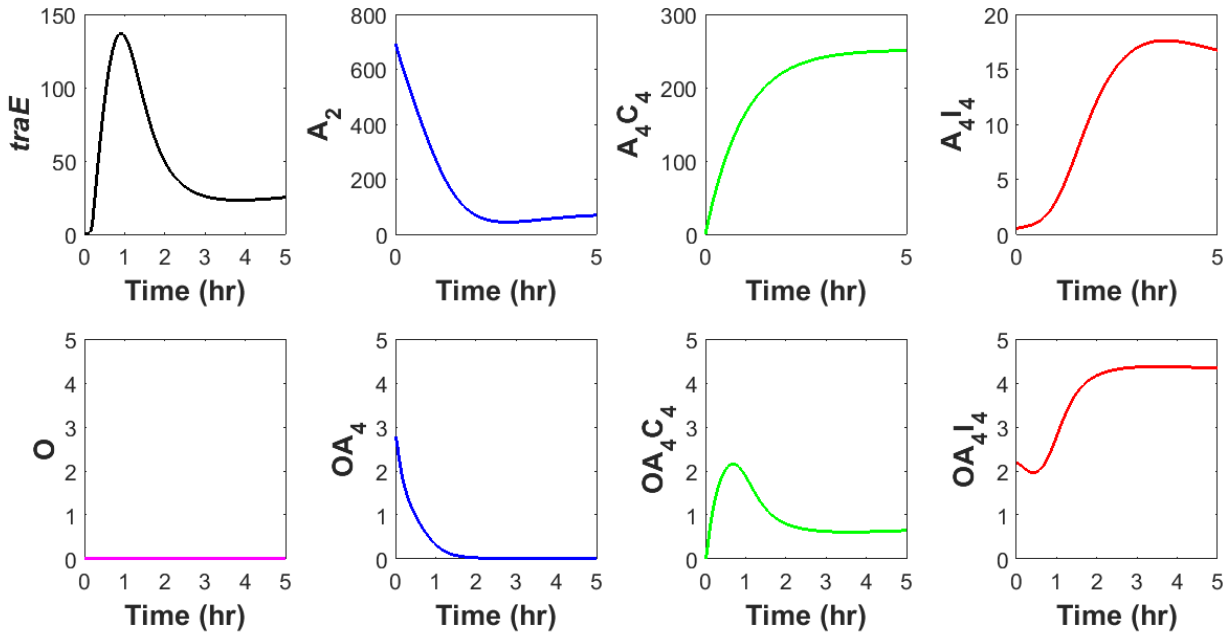

Figure S5: Dynamic simulation of the induction behavior of the conjugation operon. The deterministic model developed for pCF10 was modified to simulate the induction behavior for pAD1 and pAM373. The simulation was done keeping exogenous pheromone concentration constant and its effect on the time dynamics of *traE1*/*traE*, O, OX_4, OX_4C_4, and OX_4I_4 is shown (A) pAD1 simulated under 50ng/mL cAD1. (B) pAM373 simulated under 500ng/mL cAM373 with parameter set I (C) pAM373 simulated under 500ng/mL cAM373 with parameter set II.

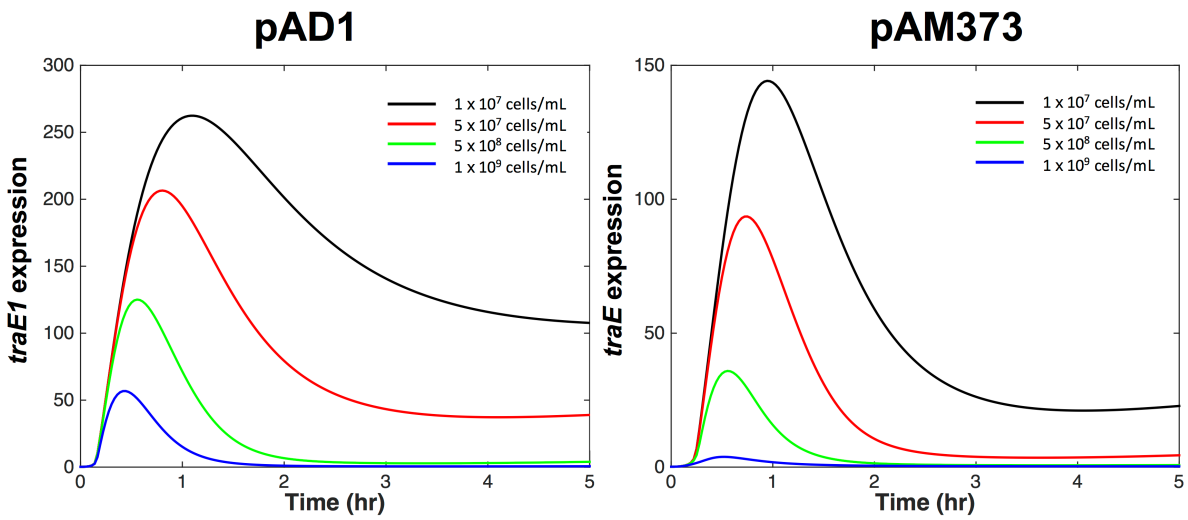

Figure S6. Effect of donor density on the on the dynamics of on induction. Dynamic simulation of the model was done keeping exogenous pheromone concentration constant and varying the donor density and its effect on the time dynamics of *traE1*/*traE* is shown. (A) pAD1 simulated under 50ng/mL cAD1. (B) pAM373 simulated under 500ng/mL cAM373 with parameter set II